Prediction of the analyzing power for $\vec{p} + {}^6$He elastic scattering at 200 MeV from $\vec{p} + {}^4$He elastic scattering at 200 MeV

Masahiro Ishii,[1,*] Yasunori Iseri,[2,†] and Masanobu Yahiro[1,‡]
[1]*Department of Physics, Graduate School of Sciences, Kyushu University, Fukuoka 819-0395, Japan*
[2]*Chiba-Keizai College, Chiba 263-0021, Japan*

(Received 6 April 2020; revised 9 January 2021; accepted 3 February 2021; published 5 April 2021)

Background: Johnson, Al-Khalili, and Tostevin constructed a theory for one-neutron halo-nucleus scattering, taking (1) the adiabatic approximation and (2) neglecting the interaction between a valence neutron and a target, and yielding a simple relationship between the elastic scattering of a halo nucleus and of its core. The core-target scattering is calculated with the reduced mass between a halo nucleus and a target, and hence is not measured with the experiment.
Purpose: Our first aim is to apply their theory for $\vec{p} + {}^6$He elastic scattering as two-neutron halo-nucleus scattering and improve the theory with (3) the eikonal approximation. Our second aim is to investigate how good the improved theory is.
Methods: An improved valence-target-cutting (VTC) theory and cluster-folding (CF) model.
Results: The improved VTC theory shows a new relation between two differential cross sections measured for $\vec{p} + {}^{4,6}$He scattering. Using the relation, we show that the analyzing power $A_y(q)$ for ^{6}He is the same as for ^{4}He. In the improved theory, the ratio of measured differential cross section for ^{4}He to that for ^{6}He determines a radius $r_{\alpha-2n}$ between ^{4}He and the center of mass of two valence neutrons; the value is $r_{\alpha-2n} = 3.54$ fm. Among the approximations (1)–(3), the approximation (2) is essential. In order to investigate the approximation (2), we apply the CF model for $\vec{p} + {}^6$He scattering at 200 MeV, where the potential between $\vec{p}$ and ^{4}He is fitted to data on $\vec{p} + {}^4$He scattering at 200 MeV. For $\vec{p} + {}^6$He scattering at 200 MeV, the CF model reproduces the measured differential cross section with no free parameter. The CF model shows that the approximation (2) is good in $0.9 \lesssim q \lesssim 2.4$ fm^{-1}, where $\hbar q$ is the transfer momentum. Using the improved theory, in $0.9 \lesssim q \lesssim 2.4$ fm^{-1}, we predict $A_y(q)$ for ^{6}He from measured $A_y(q)$ for ^{4}He.
Conclusions: The improved VTC theory shows shows that $A_y(q)$ for ^{6}He is the same as for ^{4}He.

DOI: 10.1103/PhysRevC.103.044605

I. INTRODUCTION

In the shell model, the central and spin-orbit potentials are important for understanding nuclear structure. The importance was first discovered by Mayer and Jensen. The central and spin-orbit potentials in various stable nuclei are similar to the real part of the optical potential in the $\vec{p}$ elastic scattering on the corresponding stable nuclei. The optical potentials are well determined by measured differential cross sections $d\sigma/d\Omega$ and analyzing powers A_y.

In general, the central and spin-orbit potentials in the scattering of unstable nuclei on a $\vec{p}$ target are different from the case of stable nuclei, since unstable nuclei have larger radii than the stable nuclei with the common mass number [1,2].

For scattering of ^{6}He on a $\vec{p}$ target at an incident energy $E_{\rm lab} = 71$ MeV/nucleon, the A_y was obtained in the inverse measurement [3–5]. In the experiment, the $d\sigma/d\Omega$ is measured in $1.1 \lesssim q \lesssim 2.2$ fm^{-1} ($42^\circ \lesssim \theta_{\rm c.m.} \lesssim 87^\circ$) and the A_y is in $1.0 \lesssim q \lesssim 1.9$ fm^{-1} ($37^\circ \lesssim \theta_{\rm c.m.} \lesssim 74^\circ$) [3–5], where $\hbar q$ and $\theta_{\rm c.m.}$ are the transfer momentum and the scattering angle in the center-of-mass (c.m.) frame, respectively. The measured A_y is reproduced by the the cluster-folding (CF) model [5]. It is shown in Ref. [5] that the spin-orbit part of the phenomenological optical potential is shallow and long-ranged. This problem is not solved yet.

The same measurement was made for $E_{\rm lab} = 200$ MeV/nucleon [6], since the nucleon-nucleon (NN) total cross section has a minimum around there. However, the result was shown only for $d\sigma/d\Omega$ in $1.7 \lesssim q \lesssim 2.7$ fm^{-1} ($36^\circ \lesssim \theta_{\rm c.m.} \lesssim 59^\circ$).

The $\vec{p} + {}^{4,6}$He scattering at $E_{\rm lab} = 200$ MeV/nucleon were analyzed by the Melbourne g-matrix folding model [1]. The model predicted $d\sigma/d\Omega$ and A_y for ^{6}He, but not does account for the data [7] for ^{4}He in $q \gtrsim 3.3$ fm^{-1} ($\theta_{\rm c.m.} \gtrsim 80^\circ$). *Ab initio* folding potentials based on no-core shell-model [8] were constructed and applied for $\vec{p} + {}^{4,6}$He scattering at $E_{\rm lab} = 200$ MeV/nucleon. The model reproduces the data on $d\sigma/d\Omega$ for ^{6}He, but not $d\sigma/d\Omega$ for ^{4}He in $q \gtrsim 2.5$ fm^{-1} ($\theta_{\rm c.m.} \gtrsim 60^\circ$).

Crespo and Moro calculated $d\sigma/d\Omega$ and A_y for the $\vec{p} + {}^{4,6,8}$He scattering at $E_{\rm lab} = 297$ MeV/nucleon, using the multiple scattering expansion [9]. Microscopic optical potentials derived from NN t matrix and nonlocal density was applied for the $\vec{p} + {}^4$He scattering at $E_{\rm lab} = 200$ MeV/nucleon [10],

*ishii@phys.kyushu-u.ac.jp
†iseri@chiba-kc.ac.jp
‡yahiro@phys.kyushu-u.ac.jp

and reproduced the data of Ref. [7] in $q \lesssim 4.1$ fm^{-1} ($\theta_{\rm c.m.} \lesssim 110^\circ$).

Johnson, Al-Khalili, and Tostevin constructed a theory for one-neutron halo-nucleus scattering, using (1) the adiabatic approximation and (2) neglecting the interaction between a valence neutron and a target [11]. They yield a simple relationship between the elastic scattering of a halo nucleus and of its core from a stable target. They applied the theory for ^{11}Be + ^{12}C and ^{19}C + ^{12}C scattering, since the core mass is much larger than the valence-neutron mass. Nevertheless, they found that the approximation (2) is not negligible. There is no statement on A_y in Ref. [11]. For simplicity, we refer to the theory as valence-target cutting (VTC) theory. The case of multinucleon valence halo systems is described in Ref. [12].

In Ref. [11], the differential cross section of the core-target scattering is calculated with the reduced mass μ between a halo nucleus and a target, and not measured with the experiment.

In this paper, we apply the VTC theory for a two-neutron halo nucleus scattering and improve the extended theory with (3) the eikonal approximation. Among the three approximations used, the approximation (2) is most essential for $\vec{p}+{}^6$He elastic scattering, since the core mass is comparable with the two-neutron mass. We consider $\vec{p}+{}^6$He scattering at $E_{\rm lab} =$ 71, 200 MeV/nucleon. As a second aim, we investigate how good the improved VTC theory is for the $\vec{p}+{}^6$He scattering, that is, how good the approximation (2) is for the $\vec{p}+{}^6$He scattering.

The improved VTC theory shows that $A_y(q)$ for ^{4}He is the same as $A_y(q)$ for ^{6}He. This makes it possible to determine $A_y(q)$ for ^{6}He from the data on $A_y(q)$ for ^{4}He. The ratio $F(\boldsymbol{q}/3)$ of $d\sigma/d\Omega$ for ^{6}He to that for ^{4}He is related to the wave function of ^{6}He in the improved VTC theory. This allows us to determine the radius $r_{\alpha-2n}$ between ^{4}He and the center-of-mass of valence two neutrons from $F(\boldsymbol{q}/3)$.

Using the CF model, we confirm that the approximation (2) is good in $0.9 \lesssim q \lesssim 2.4$ fm^{-1} for $E_{\rm lab} = 200$ MeV/nucleon, but good only in the vicinity of $q = 0.9$ fm^{-1} for $E_{\rm lab} = 71$ MeV/nucleon.

The improved VTC theory and the results are shown in Sec. II. The CF model is explained and its results are shown in Sec. III. Section IV is devoted to a summary.

II. IMPROVED VTC THEORY AND ITS RESULTS

We extend the VTC theory for ^{6}He elastic scattering on a target $\vec{p}$ at $E_{\rm lab} = 71$ and 200 MeV/nucleon as two-neutron halo-nucleus scattering. For this purpose, we start with the $p + n_1 + n_2 + {}^4$He four-body model; see Fig. 1 for two sets of coordinates in the four-body system.

The four-body Hamiltonian is

$$H = -\frac{\hbar^2}{2\mu_6}\nabla_R^2 + U + H_6, \tag{1}$$

$$U = U_{pn_1}(r_{pn_1}) + U_{pn_2}(r_{pn_2}) + U_{p\alpha}(r_{p\alpha}) + V_{p\alpha}^{\rm Coul}(r_{p\alpha}), \tag{2}$$

where μ_6 is the reduce mass between $\vec{p}$ and ^{6}He and the Hamiltonian H_6 of ^{6}He is described by the $n_1 + n_2 + {}^4$He three-body model. The coordinates $\boldsymbol{r}_{p\gamma}$ for $\gamma = n_1, n_2, \alpha$ are shown in Fig. 1 (a). The $U_{p\gamma}$ is the nuclear interaction between $\vec{p}$ and γ.

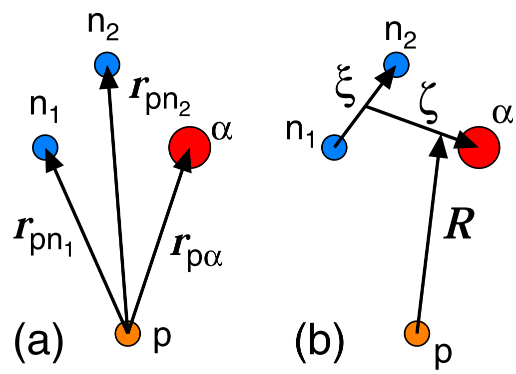

FIG. 1. Two sets of coordinates in four-body model.

The exact T matrix of the elastic scattering is

$$T = \langle e^{i\boldsymbol{k}'\cdot\boldsymbol{R}}\Phi|\, U\, |\, \Psi\rangle \tag{3}$$

for the total wave function Ψ, the incident and final momenta, $\hbar\boldsymbol{k}$ and $\hbar\boldsymbol{k}'$. The ground state $\Phi(\xi,\zeta)$ of ^{6}He has an energy ε_0.

We take the adiabatic approximation ($H_6 \approx \varepsilon_0$) for H and neglect the interactions U_{pn_1} and U_{pn_2}. The resulting Hamiltonian is

$$H_{\rm AD} = -\frac{\hbar^2}{2\mu_6}\nabla_R^2 + U_{p\alpha}(r_{p\alpha}) + V_{p\alpha}^{\rm Coul}(r_{p\alpha}) + \varepsilon_0. \tag{4}$$

In $H_{\rm AD}$, ζ is a constant, because of no derivative with respect to ζ. We then get $\nabla_R^2 = \nabla_{r_{p\alpha}}^2$ for $\boldsymbol{R} = \boldsymbol{r}_{p\alpha} - \zeta/3$. Eventually, we get

$$H_{\rm AD} = -\frac{\hbar^2}{2\mu_6}\nabla_{r_{p\alpha}}^2 + U_{p\alpha}(r_{p\alpha}) + V_{p\alpha}^{\rm Coul}(r_{p\alpha}) + \varepsilon_0. \tag{5}$$

The solution $\Psi_{\rm AD}$ to the Schrödinger equation $[E_{\rm c.m.} - H_{\rm AD}]\Psi_{\rm AD} = 0$ is

$$\begin{aligned}\Psi_{\rm AD} &= \frac{i\varepsilon}{E_{\rm c.m.} - H_{\rm AD} + i\varepsilon} e^{i\boldsymbol{k}\cdot\boldsymbol{R}}\Phi \\ &= \frac{i\varepsilon}{E_{\rm c.m.} - H_{\rm AD} + i\varepsilon} e^{i\boldsymbol{k}\cdot\boldsymbol{r}_{p\alpha}} e^{-i\boldsymbol{k}\cdot\zeta/3}\Phi \\ &= e^{-i\boldsymbol{k}\cdot\zeta/3}\Phi \frac{i\varepsilon}{E_{\rm c.m.} - H_{\rm AD} + i\varepsilon} e^{i\boldsymbol{k}\cdot\boldsymbol{r}_{p\alpha}} \\ &= e^{-i\boldsymbol{k}\cdot\zeta/3}\Phi\chi_{\boldsymbol{k}}(\boldsymbol{r}_{p\alpha})\end{aligned} \tag{6}$$

with the distorting wave function

$$\chi_{\boldsymbol{k}}(\boldsymbol{r}_{p\alpha}) = \frac{i\varepsilon}{E_{\rm c.m.} - H_{\rm AD} + i\varepsilon} e^{ik\boldsymbol{r}_{p\alpha}} \tag{7}$$

for infinitesimally small ε and the incident energy $E_{\rm cm} = \hbar^2k^2/(2\mu_6)$ in the center of mass (c.m.) system. Inserting Eq. (6) in Eq. (3), we can obtain an approximate T matrix $T_{\rm AD}$ as

$$\begin{aligned}T_{\rm AD} &= \langle e^{i\boldsymbol{k}'\boldsymbol{R}}\Phi|\, U_{p\alpha} + V_{p\alpha}^{\rm Coul}(r_{p\alpha})|e^{-ik\zeta/3}\Phi\chi_{\boldsymbol{k}}(\boldsymbol{r}_{p\alpha})\rangle \\ &= F((\kappa' - \kappa)/3)\langle e^{i\boldsymbol{k}'\cdot\boldsymbol{r}_{p\alpha}}|U_{p\alpha} + V_{p\alpha}^{\rm Coul}|\chi_{\boldsymbol{k}}(\boldsymbol{r}_{p\alpha})\rangle_{\boldsymbol{r}_{p\alpha}},\end{aligned} \tag{8}$$

where the subscript $\boldsymbol{r}_{p\alpha}$ shows the integral over $\boldsymbol{r}_{p\alpha}$. The $F(\boldsymbol{Q})$ as a function of $\boldsymbol{Q} \equiv (\boldsymbol{\kappa}' - \boldsymbol{\kappa}) = \boldsymbol{q}/3$ is the form factor defined by

$$F(\boldsymbol{Q}) \equiv F((\boldsymbol{\kappa}' - \boldsymbol{\kappa})/3) = \langle e^{i(\boldsymbol{k}'-\boldsymbol{k})\cdot\zeta/3}|\Phi|^2\rangle_{\zeta\xi}, \tag{9}$$

where the subscript $\zeta\xi$ shows the integral over ζ and ξ.

The $\chi_{\boldsymbol{k}}(\boldsymbol{r}_{p\alpha})$ is the distorting wave function between $\vec{p}$ and ^{4}He with the reduced mass μ_6, and not the distorting wave function of the $\vec{p}+{}^4$He elastic scattering with the reduced mass μ_4 between $\vec{p}$ and ^{4}He.

Using Eq. (8), we can get the differential cross section of $\vec{p}+{}^6$He scattering as

$$\left(\frac{d\sigma}{d\Omega}\right)_{p+{}^6\mathrm{He}} = |F(\boldsymbol{Q})|^2\left(\frac{d\sigma}{d\Omega}\right)^{\mathrm{point}}. \tag{10}$$

In the limit of $F(\boldsymbol{Q}) = 1$, the distance between ^{6}He and the c.m. of two valence neutrons tends to zero. In this sense, $(\frac{d\sigma}{d\Omega})^{\mathrm{point}}$ is called the point cross section. The equation is a four-body version of Ref. [11].

The $(\frac{d\sigma}{d\Omega})^{\mathrm{point}}$ is calculated in Ref. [11] for one-neutron halo-nucleus scattering, since the $(\frac{d\sigma}{d\Omega})^{\mathrm{point}}$ cannot be measured with experiments.

In order to determine $|F(\boldsymbol{Q})|$ from experimental data on $p+{}^{4,6}$He scattering, we find a relationship between the $(d\sigma/d\Omega)^{\mathrm{point}}$ and the differential cross section $(d\sigma/d\Omega)_{p+{}^4\mathrm{He}}$ for $p+{}^4$He elastic scattering with μ_4.

In the c.m. system, the velocity v_A is defined with $\hbar k_A = v_A\mu_A$ for $A = 4$ or 6, and hence

$$E^A_{\mathrm{c.m.}} = \frac{(\hbar k_A)^2}{2\mu_A} = \mu_A\frac{v_A^2}{2} = \frac{A}{A+1}M_N\frac{v_A^2}{2} \tag{11}$$

for nucleon mass M_N. In the laboratory system, the energy E^A_{lab} per nucleon is described with the velocity v^A_{lab} as

$$E^A_{\mathrm{lab}} = M_N\frac{\left(v^A_{\mathrm{lab}}\right)^2}{2}. \tag{12}$$

The transform from $E^A_{\mathrm{c.m.}}$ to the incident energy AE^A_{lab} leads to

$$E^A_{\mathrm{c.m.}} = \frac{1}{A+1}AE^A_{\mathrm{lab}} = \frac{A}{A+1}M_N\frac{\left(v^A_{\mathrm{lab}}\right)^2}{2}. \tag{13}$$

Comparing Eq. (11) with Eq. (13), we show that

$$v_A = v^A_{\mathrm{lab}}. \tag{14}$$

This means that the velocity v defined with $\hbar k_A = v_A\mu_A$ in the c.m. system is the same as the the velocity v^A_{lab} in the laboratory system.

From now on, we consider the case of $v \equiv v_4 = v_6$. This case corresponds to taking the case of

$$E^4_{\mathrm{lab}} = E^6_{\mathrm{lab}} = M_N\frac{v_{\mathrm{lab}}^2}{2} = M_N\frac{v^2}{2}, \tag{15}$$

because of Eqs. (12) and (14).

Now we improve Eq. (10) in order to determine $|F(\boldsymbol{Q})|$ from experimental data on $\vec{p}+{}^{4,6}$He scattering at the same E_{lab}. Using the eikonal approximation for the $\vec{p}+{}^4$He scattering in the center-of-mass system, we get the scattering amplitude $f_{p\alpha}$ as

$$f_{p\alpha} = \frac{i\mu_4 v}{2\pi\hbar}\int d\boldsymbol{b}\, e^{-i\boldsymbol{q}\cdot\boldsymbol{b}}(1-e^{i\chi(\boldsymbol{b})}) \tag{16}$$

with the phase shift function

$$\chi(\boldsymbol{b}) = -\frac{1}{\hbar v}\int_{-\infty}^{\infty} dz\,[U_{p\alpha}(\boldsymbol{b},z) + V^{\mathrm{Coul}}_{p\alpha}(\boldsymbol{b},z)F(\boldsymbol{r}_{p\alpha})], \tag{17}$$

where $\boldsymbol{r}_{p\alpha} \equiv (\boldsymbol{b}, z)$ and the screened Coulomb potential $V^{\mathrm{Coul}}_{p\alpha}(z,\boldsymbol{b})F(\boldsymbol{r}_{p\alpha})$ has been used instead of $V^{\mathrm{Coul}}_{p\alpha}(\boldsymbol{b}, z)$. Glauber shows how to treat the screening function $F(\boldsymbol{r}_{p\alpha})$ below Eq. (117) in Ref. [13]. The spin-orbit part of $U_{p\alpha}(z,\boldsymbol{b})$ is approximated as

$$\begin{aligned} U^{\mathrm{LS}}_{p\alpha}(r_{p\alpha})\boldsymbol{\ell}_{p\alpha}\boldsymbol{\sigma}_p &\approx U^{\mathrm{LS}}_{p\alpha}(r_{p\alpha})(\hbar\boldsymbol{k}_4\times\boldsymbol{r}_{p\alpha})\boldsymbol{\sigma}_p \\ &= U^{\mathrm{LS}}_{p\alpha}(r_{p\alpha})(\hbar\boldsymbol{k}_4\times\boldsymbol{r}_{p\alpha})\boldsymbol{\sigma}^{(y)}_p \\ &= U^{\mathrm{LS}}_{p\alpha}(r_{p\alpha})(\mu_4\boldsymbol{v}\times\boldsymbol{r}_{p\alpha})\boldsymbol{\sigma}^{(y)}_p, \end{aligned} \tag{18}$$

where $\boldsymbol{v}\times\boldsymbol{r}_{p\alpha} = \boldsymbol{v}\times\boldsymbol{b} = vb\boldsymbol{e}_y$ since $\boldsymbol{v}$ is in the z direction and the unit vector $\boldsymbol{e}_y$ is in the y direction, i.e., the vertical direction of the scattering plane. It is possible to define $\boldsymbol{\sigma}^{(y)}_p$ as $\boldsymbol{\sigma}^{(y)}_p = \mathrm{diag}(1,-1)$; namely, $\boldsymbol{\ell}_{p\alpha}\cdot\boldsymbol{\sigma}_p = \mu_4 vb$ for proton having up-spin and, $\boldsymbol{\ell}_{p\alpha}\cdot\boldsymbol{\sigma}_p = -\mu_4 vb$ for proton having down-spin. The χ^+ for up-spin is decoupled from the χ^- for down-spin. This property is essential for the derivation of Eq. (24), as shown later.

Equation (18) shows that $\chi(\boldsymbol{b})$ depends on the reduced mass, i.e., $\chi(\boldsymbol{b}) = \chi(\boldsymbol{b},\mu_4)$. Note that the reduced-mass dependence of $\chi(\boldsymbol{b},\mu_4)$ comes from the LS potential only. Under the the eikonal approximation, the $(\frac{d\sigma}{d\Omega})^{\mathrm{point}}$ reads

$$\begin{aligned} \left(\frac{d\sigma}{d\Omega}\right)^{\mathrm{point}} &= \left|\frac{i\mu_6 v}{2\pi\hbar}\int d\boldsymbol{b}\, e^{-i\boldsymbol{q}\cdot\boldsymbol{b}}(1-e^{i\chi(\boldsymbol{b},\mu_6)})\right|^2 \\ &\approx \left|\frac{i\mu_6 v}{2\pi\hbar}\int d\boldsymbol{b}\, e^{-i\boldsymbol{q}\cdot\boldsymbol{b}}(1-e^{i\chi(\boldsymbol{b},\mu_4)})\right|^2. \end{aligned} \tag{19}$$

The replacement from $\chi(\boldsymbol{b},\mu_6)$ to $\chi(\boldsymbol{b},\mu_4)$ is good approximation, because of $\mu_6/\mu_4 \approx 1$. The replacement hardly changes the difference cross section and A_y.

This leads to

$$\left(\frac{d\sigma}{d\Omega}\right)^{\mathrm{point}} = \left(\frac{\mu_6}{\mu_4}\right)^2\left|f_{p\alpha}\right|^2 = \left(\frac{\mu_6}{\mu_4}\right)^2\left(\frac{d\sigma}{d\Omega}\right)_{p+{}^6\mathrm{He}}. \tag{20}$$

In the c.m. system, we then obtain

$$\left(\frac{d\sigma}{d\Omega}\right)_{p+{}^6\mathrm{He}} = |F(\boldsymbol{Q})|^2\left(\frac{d\sigma}{d\Omega}\right)_{p+{}^4\mathrm{He}}\left(\frac{\mu_6}{\mu_4}\right)^2 \tag{21}$$

from Eqs. (10) and (20), where the two differential cross sections are for $\vec{p}+{}^{4,6}$He scattering at a common v, i.e., a common E_{lab}. This new relation (21) allows us to determine $|F(\boldsymbol{Q})|$ from two differential cross sections measured for $\vec{p}+{}^{4,6}$He scattering at a common E_{lab}.

The derivation from Eqs. (5) to (21) is the same for incident proton having up-spin (+) and incident proton down-spin (−), although $U_{p\alpha}$ for incident proton having up-spin (+) is different from that for incident proton having down-spin (−).

Eventually, we can get

$$\left(\frac{d\sigma}{d\Omega}\right)^{+}_{p+{}^6\mathrm{He}} = |F(\boldsymbol{Q})|^2 \left(\frac{d\sigma}{d\Omega}\right)^{+}_{p+{}^4\mathrm{He}} \left(\frac{\mu_6}{\mu_4}\right)^2 \tag{22}$$

and

$$\left(\frac{d\sigma}{d\Omega}\right)^{-}_{p+{}^6\mathrm{He}} = |F(\boldsymbol{Q})|^2 \left(\frac{d\sigma}{d\Omega}\right)^{-}_{p+{}^4\mathrm{He}} \left(\frac{\mu_6}{\mu_4}\right)^2, \tag{23}$$

where $F(\boldsymbol{Q})$ is common between incident proton having up-spin (+) and incident proton down-spin (−) since $F(\boldsymbol{Q})$ is not related to the spin of incident proton.

Using Eqs. (22) and (23), one can get a relation for the analyzing power A_y^6 for ^{6}He as

$$\begin{aligned} A_y^6 &\equiv \frac{\left(\frac{d\sigma}{d\Omega}\right)^{+}_{p+{}^6\mathrm{He}} - \left(\frac{d\sigma}{d\Omega}\right)^{-}_{p+{}^6\mathrm{He}}}{\left(\frac{d\sigma}{d\Omega}\right)^{+}_{p+{}^6\mathrm{He}} + \left(\frac{d\sigma}{d\Omega}\right)^{-}_{p+{}^6\mathrm{He}}} \\ &= \frac{\left(\frac{d\sigma}{d\Omega}\right)^{+}_{p+{}^4\mathrm{He}} - \left(\frac{d\sigma}{d\Omega}\right)^{-}_{p+{}^4\mathrm{He}}}{\left(\frac{d\sigma}{d\Omega}\right)^{+}_{p+{}^4\mathrm{He}} + \left(\frac{d\sigma}{d\Omega}\right)^{-}_{p+{}^4\mathrm{He}}} \equiv A_y^4. \end{aligned} \tag{24}$$

This equation shows that $A_y(q)^6 = A_y(q)^4$ in the improved VTC theory. In fact, Eq. (24) is well satisfied in A_y for 71 MeV; see Fig. 4.

The relation (21) between $(\frac{d\sigma}{d\Omega})^{E_{\rm lab}}_{p+{}^6\mathrm{He}}$ and $(\frac{d\sigma}{d\Omega})^{E_{\rm lab}}_{p+{}^4\mathrm{He}}$ is good, when the eikonal and adiabatic approximations are good and $U_{pn_1} = U_{pn_2} = 0$. It is shown in Ref. [14] that the eikonal and adiabatic approximations are good for a few hundred MeV. The approximation $U_{pn_1} = U_{pn_2} = 0$ is good in $0.9 \lesssim q \lesssim 2.4$ fm^{-1} for 200 MeV as shown in Sec. III B, but good only near $q = 0.9$ fm^{-1} for 71 MeV as mentioned in Sec. III C.

A. Determination of |F| from measured differential cross sections for $\vec{p} + {}^{4,6}$He scattering

Using Eq. (21), we can determine $|F(Q)|$ from experimental data on the cross sections of $p + {}^{4,6}$He scattering at the same $E_{\rm lab}$, when the most essential condition $U_{pn_1} = U_{pn_2} = 0$ is good and the angular momentum between n_1 and n_2 is zero.

As for $E_{\rm lab} = 200$ MeV/nucleon, the data are available in Ref. [7] for ^{4}He and in Ref. [6] for ^{6}He. As for $E_{\rm lab} = 71$ MeV/nucleon, the data are available in Refs. [5,15] for ^{6}He, but not for ^{4}He. We then take the data [16] on $\vec{p} + {}^4$He scattering at $E_{\rm lab} = 72$ MeV/nucleon. The resulting $|F(Q)|$ is smooth, as shown in Fig. 2. The approximation $U_{pn_1} = U_{pn_2} = 0$ is good in $0.9 \lesssim q \lesssim 2.4$ fm^{-1} for 200 MeV as shown in Sec. III B, but good only in the vicinity of $q = 0.9$ fm^{-1} for 71 MeV as mentioned in Sec. III C. In Fig. 2, the resulting $|F(Q)|$ is thus reliable in $0.3 \lesssim Q \lesssim 0.8$ fm^{-1}.

The Fourier transform $|F(\zeta)|$ of $|F(Q)|$ is a function of ζ. We then assume that the potential between ^{4}He and the center of mass of n_1 and n_2 is a one-range Gauss function $V(\zeta)$, and can obtain $|F(Q)|$ by solving the Schrödinger equation with the potential. The solid line denotes a result of $V(\zeta) = -25\exp[-(\zeta/1.41)^2]$, and reproduces the experimental $|F(Q)|$ for 200 MeV. The resulting radius between ^{4}He and the center of mass of n_1 and n_2 is 3.54 fm. The corresponding binding energy is 0.172 MeV.

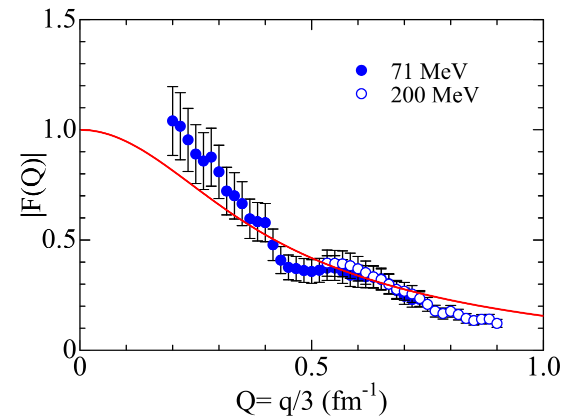

FIG. 2. Q dependence of $|F|$. The solid (open) circles are the result determined from the experimental data at 71 (200) MeV. The solid line is a result of $V(\zeta) = -25\exp[-(\zeta/1.41)^2]$. Experimental data are taken from Refs. [5,15,16] for 71 MeV and Refs. [6,7] for 200 MeV.

B. Model independent prediction on A_y for $\vec{p} + {}^{4,6}$He scattering at 200 MeV

When p is polarized, the factor $|F(\hbar(\boldsymbol{\kappa}' - \boldsymbol{\kappa}))/3|\mu_6/\mu_4$ is common between the cross section for the incident proton having up-spin and that for the proton having down-spin. This means that the vector analyzing $A_y(q)$ for $\vec{p} + {}^6$He scattering is the same as $A_y(q)$ for $\vec{p} + {}^4$He, when the condition $U_{pn_1} = U_{pn_2} = 0$ is good. As mentioned later in Sec. III B, the condition is well satisfied in $0.9 \lesssim q \lesssim 2.4$ fm^{-1}.

We make a model-independent prediction on $A_y(q)$ for ^{6}He by using Eq. (24). The measured $A_y(q)$ of Ref. [7] for ^{4}He is transformed into $A_y(\theta_{\rm c.m.})$.

Figure 3 shows the predicted $A_y(\theta_{\rm c.m.})$ for ^{6}He. The predicted $A_y(\theta_{\rm c.m.})$ is reliable in $20^\circ \lesssim \theta_{\rm c.m.} \lesssim 55^\circ$ $(0.9 \lesssim q \lesssim 2.4$ fm$^{-1})$. The reliable prediction in $20^\circ \lesssim \theta_{\rm c.m.} \lesssim 55^\circ$ is denoted by closed circles. It should be noted that our prediction shown by open circles are not good.

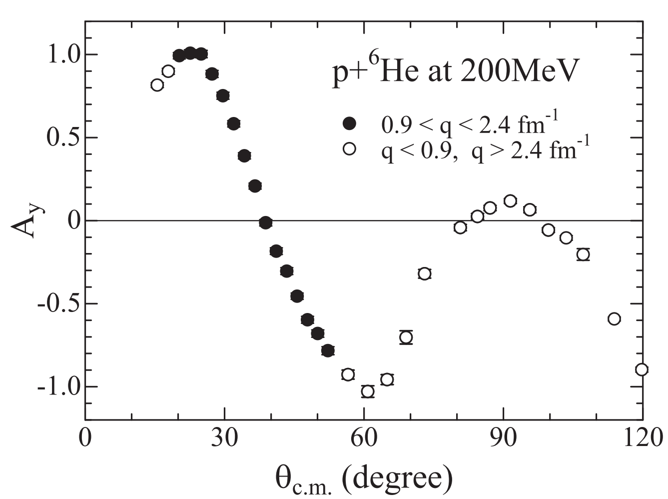

FIG. 3. $\theta_{\rm c.m.}$ dependence of predicted A_y for $\vec{p} + {}^6$He scattering at 200 MeV. See the text for closed and open circles.

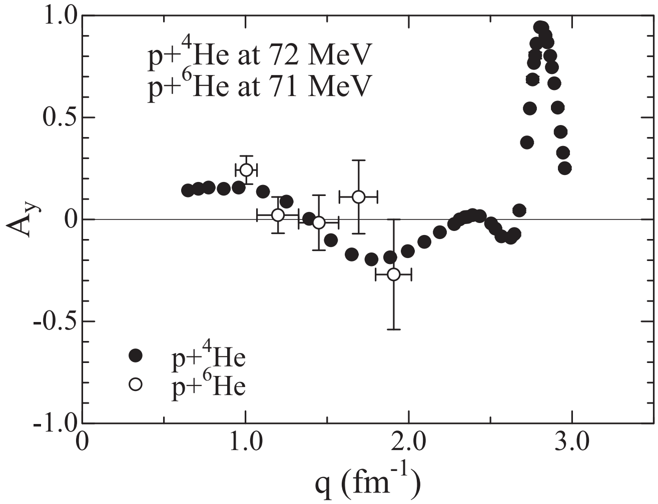

FIG. 4. q dependence of measured A_y (closed circles) for $\vec{p}+{}^4$He scattering at $E_{\rm lab}=72$ MeV and measured A_y (open circles) for $\vec{p}+{}^6$He scattering at $E_{\rm lab}=71$ MeV. Data are taken from Ref. [5] for ^{6}He and Ref. [16] for ^{4}He.

C. A_y for 71 MeV

Figure 4 shows q dependence of A_y measured for $\vec{p}+{}^4$He scattering at $E_{\rm lab}=72$ MeV/nucleon and that for $\vec{p}+{}^6$He scattering at $E_{\rm lab}=71$ MeV/nucleon. The A_y for ^{6}He is close to that for ^{4}He, except for a data at $q=1.71$ fm^{-1}. The property can be analyzed quantitatively by the Jensen-Shannon (JS) divergence [17]. We show the analysis in the Appendix, since the analysis is new but has recently been used by LIGO Scientific and Virgo Collaborations [18].

III. CLUSTER-FOLDING MODEL

In order to investigate the approximation (2), we use the CF model for $\vec{p}+{}^6$He scattering at 200 MeV, where the potential between $\vec{p}$ and ^{4}He is fitted to data on $\vec{p}+{}^4$He scattering at 200 MeV. The CF model reproduces the differential cross section for $\vec{p}+{}^6$He scattering with no free parameter. We then predict A_y.

We consider the cluster folding (CF) model for the $\vec{p}+{}^6$He at $E_{\rm lab}=200$ MeV. In addition, we recalculate the scattering for $E_{\rm lab}=71$ MeV in order to obtain F.

In the cluster model, the nuclear potential $U_{\rm CF}(R)$ between $\vec{p}$ and ^{6}He is defined as

$$U_{\rm CF}(R)=\int U_{pn_1}\,\rho_n^{\rm CF}(r_1)\,d\boldsymbol{r}_1+\int U_{pn_2}\,\rho_n^{\rm CF}(r_2)\,d\boldsymbol{r}_2+\int U_{p\alpha}\,\rho_\alpha^{\rm CF}(r_\alpha)\,d\boldsymbol{r}_\alpha \tag{25}$$

with

$$U_{pn_1}=U_{pn}^0(r_{pn_1})+U_{pn}^{\rm LS}(r_{pn_1})\boldsymbol{\ell}_{pn_1}(\boldsymbol{\sigma}_p+\boldsymbol{\sigma}_{n_1}), \tag{26}$$

$$U_{pn_2}=U_{pn}^0(r_{pn_2})+U_{pn}^{\rm LS}(r_{pn_2})\boldsymbol{\ell}_{pn_2}(\boldsymbol{\sigma}_p+\boldsymbol{\sigma}_{n_2}), \tag{27}$$

$$U_{p\alpha}=U_{p\alpha}^0(r_{p\alpha})+U_{p\alpha}^{\rm LS}(r_{p\alpha})\boldsymbol{\ell}_{p\alpha}\boldsymbol{\sigma}_p, \tag{28}$$

where the coordinates $\boldsymbol{r}_1$, $\boldsymbol{r}_2$, and $\boldsymbol{r}_\alpha$ are the position vectors of n_1, n_2, and the α core from the center of mass of ^{6}He, respectively, and $\rho_n^{\rm CF}$ and $\rho_\alpha^{\rm CF}$ are the neutron and α densities, respectively. These densities of ^{6}He are calculated with αnn OCM in Refs. [19,20].

Following Ref. [5], we can rewrite the $U_{\rm CF}(R)$ into

$$U_{\rm CF}=U_0^{\rm CF}(R)+U_{\rm LS}^{\rm CF}(R)\boldsymbol{L}\boldsymbol{\sigma}_p \tag{29}$$

with the central part

$$U_0^{\rm CF}(R)=2\int U_{pn}^0(|\boldsymbol{r}_1-\boldsymbol{R}|)\,\rho_n^{\rm CF}(r_1)\,d\boldsymbol{r}_1+\int U_{p\alpha}^0(|\boldsymbol{r}_\alpha-\boldsymbol{R}|)\,\rho_\alpha^{\rm CF}(r_\alpha)\,d\boldsymbol{r}_\alpha \tag{30}$$

and the spin-orbit part

$$U_{\rm LS}^{\rm CF}(R)=\frac{1}{3}\int U_{pn}^{\rm LS}(|\boldsymbol{r}_1-\boldsymbol{R}|)\left\{1-\frac{\boldsymbol{r}_1\cdot\boldsymbol{R}}{R^2}\right\}\rho_n^{\rm CF}(r_1)\,d\boldsymbol{r}_1+\frac{2}{3}\int U_{p\alpha}^{\rm LS}(|\boldsymbol{r}_\alpha-\boldsymbol{R}|)\left\{1-\frac{\boldsymbol{r}_\alpha\cdot\boldsymbol{R}}{R^2}\right\}\rho_\alpha^{\rm CF}(r_\alpha)\,d\boldsymbol{r}_\alpha. \tag{31}$$

The $U_{p\alpha}$ is the optical potential (OP), and U_{pn_1} and U_{pn_1} are the CEG [21–23]. The g matrix, derived from the Hamada-Johnston potential [24], is successful in reproducing the data on $\vec{p}$ elastic scattering from many nuclei in a wide range of incident energies, $E_{\rm lab}=20$–200 MeV [21–23]. For $\vec{p}+{}^6$He elastic scattering at 71 MeV, the CF model well reproduces the data on differential cross sections and A_y [5].

A. Potential fitting of $\vec{p}+{}^4$He scattering and results of CF model $\vec{p}+{}^6$He scattering

We now fit the OP potential $U_{p\alpha}$ to data [7] for $\vec{p}+{}^4$He scattering at $E_{\rm lab}=200$ MeV with a Woods-Saxon form:

$$U_{p\alpha}=-V_0\,f_r(r_{p\alpha})-i\,W_0\,f_i(r_{p\alpha})+4i\,a_{id}\,W_{id}\,\frac{d}{dr_{p\alpha}}f_{id}(r_{p\alpha})+V_s\,\frac{2}{r_{p\alpha}}\,\frac{d}{dR}f_s(r_{p\alpha})\,\boldsymbol{\ell}_{p\alpha}\boldsymbol{\sigma}_p \tag{32}$$

with

$$f_x(r_{p\alpha})=\left[1+\exp\left(\frac{r_{p\alpha}-r_xA^{1/3}}{a_x}\right)\right]^{-1} \tag{33}$$

for $x=r,i,id,s$, where $\boldsymbol{\sigma}_p$ stands for the Pauli spin operator of an incident proton. The Coulomb potential between the proton and ^{4}He (^{6}He) is obtained from the uniformly charged sphere with the radius $1.4A^{1/3}$, where $A=4$ for ^{4}He and $A=6$ for ^{6}He.

The best-fit potential parameters are obtained by minimizing the χ^2 values of $d\sigma/d\Omega$ and A_y. The resulting parameter set is tabulated in Table I, together with the case of $E_{\rm lab}=72$ MeV of Ref. [5].

First of all, we briefly shows results of the OP and the CF model in Fig. 5. The left panel shows that our fitting is good for $\vec{p}+{}^4$He scattering at $E_{\rm lab}=200$ MeV. The right panel indicates that the CF model reproduces $\vec{p}+{}^6$He scattering at $E_{\rm lab}=200$ MeV/nucleon and that the condition $U_{pn_1}=U_{pn_2}=0$ is good for $d\sigma/d\Omega$ and A_y in $\theta_{\rm c.m.}\lesssim 52^\circ$. Now we

TABLE I. Parameters of the optical potentials for $\vec{p}+{}^4$He scattering at $E_{\rm lab}=200$ MeV/nucleon. For 72 MeV/nucleon, the parameter set is taken from Ref. [5].

	(MeV)	V_0 (MeV)	r_r (fm)	a_r (fm)	W_0 (MeV)	r_i (fm)	a_i (fm)	W_{id} (MeV)	r_{id} (fm)	a_{id} (fm)	V_s (MeV)	r_s (fm)	a_s (fm)
$p+{}^4$He	200	−26.528	0.7839	0.1446	17.098	1.205	0.5268	–	–	–	6.689	0.8215	0.2641
$p+{}^4$He	72	54.87	0.8566	0.09600	–	–	–	31.97	1.125	0.2811	3.925	0.8563	0.4914

predict A_y for $\vec{p}+{}^6$He scattering at $E_{\rm lab}=200$ MeV/nucleon, using the CF model.

Further analyses based on the improved VTC theory are made below by using q instead of $\theta_{\rm c.m.}$.

B. Model-dependent prediction on A_y for $\vec{p}+{}^{4,6}$He scattering at $E_{\rm lab}=200$ MeV/nucleon

Figure 6 shows q dependence of $d\sigma/d\Omega$ for $\vec{p}+{}^{4,6}$He scattering at $E_{\rm lab}=200$ MeV/nucleon in the upper panel and the form factor $|F(Q)|$ in the lower panel. In the upper panel, the CF model (solid line) reproduces the data [6] for $\vec{p}+{}^6$He scattering at $E_{\rm lab}=200$ MeV/nucleon with no free parameter. In the lower panel, the solid line denotes the $|F(Q)|$ calculated with the CF-folding model, while U_{pn_1} and U_{pn_2} are switched off in the dashed line. The difference between the two lines shows that effects of U_{pn_1} and U_{pn_2} are small in the region $0.3 \lesssim Q \lesssim 0.8$ fm^{-1} ($0.9 \lesssim q \lesssim 2.4$ fm^{-1}).

Figure 7 shows q dependence of A_y for $\vec{p}+{}^6$H scattering. The solid line denotes the A_y calculated with the CF-folding model, while U_{pn_1} and U_{pn_2} are switched off in the dashed line. The difference between the solid and dashed lines show that the condition $U_{pn_1}=U_{pn_2}=0$ is good in $q \lesssim 2.4$ fm^{-1}. Eventually, the condition is good in $0.9 \lesssim q \lesssim 2.4$ fm^{-1}, when we see both $d\sigma/d\Omega$ and A_y.

Now we predict A_y for $\vec{p}+{}^6$He scattering at $E_{\rm lab}=200$ MeV/nucleon, using the CF model. In $0.9 \lesssim q \lesssim 2.4$ fm^{-1}, open circles are the A_y for ^{6}He derived from the measured A_y of Ref. [7] for ^{4}He. The CF model reproduces the derived A_y in $0.9 \lesssim q \lesssim 2.0$ fm^{-1}.

C. CF results on $d\sigma/d\Omega$ and A_y for 71 MeV/nucleon

Figure 8 shows the results of the CF-model for $d\sigma/d\Omega$ and A_y of $\vec{p}+{}^6$He scattering at $E_{\rm lab}=71$ MeV/nucleon in the upper and middle panels. The CF model reproduces the data [4,5] with no free parameter. The upper and middle panels also show the results of the best optical potential for $d\sigma/d\Omega$ and A_y of $\vec{p}+{}^4$He scattering at $E_{\rm lab}=72$ MeV/nucleon.

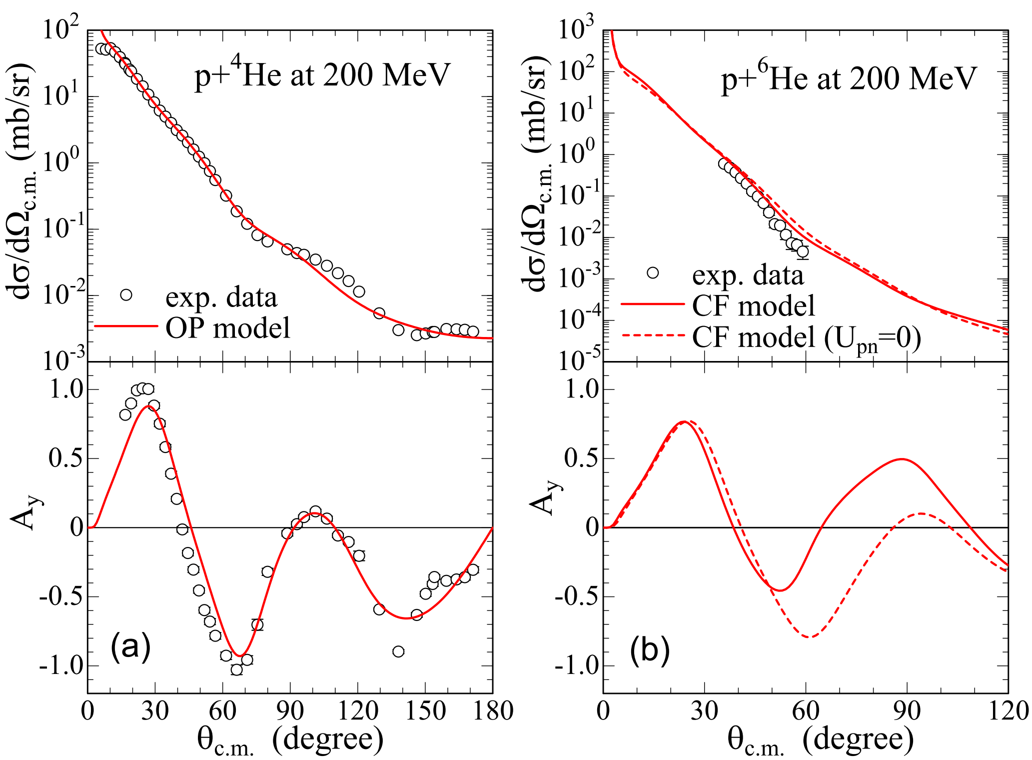

FIG. 5. $\theta_{\rm c.m.}$ dependence of $d\sigma/d\Omega$ and A_y for $\vec{p}+{}^{4,6}$He scattering at $E_{\rm lab}=200$ MeV/nucleon. In the left panel, the solid line is a result of our fitting based on the optical potential model (OPM). In the right panel, the solid and dashed lines denote results of CF model (CFM) with and without U_{pn_1} and U_{pn_2}, respectively. Experimental data are taken from Ref. [7] for ^{4}He and Ref [6] for ^{6}He.

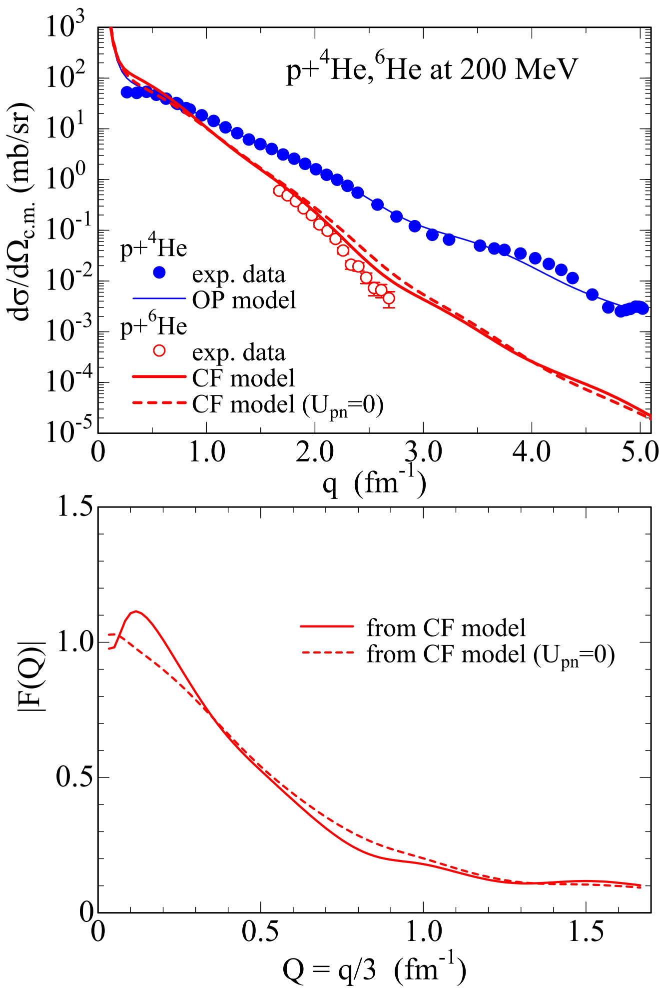

FIG. 6. q dependence of $d\sigma/d\Omega$ for $\vec{p}+{}^{4,6}$He scattering at $E_{\rm lab} = 200$ MeV/nucleon in the upper panel and the form factor $|F(Q)|$ in the lower panel. Experimental data are taken from Ref. [7] for $\vec{p}+{}^4$He scattering and Ref. [6] for $\vec{p}+{}^6$He scattering.

The lower panel shows the $|F(Q)|$ calculated with the CF model. The difference between the solid and dashed lines indicates that the condition $U_{pn_1} = U_{pn_2} = 0$ is good only in the vicinity of $Q = 0.3$ fm^{-1}.

IV. SUMMARY

In order to make the model-independent prediction for $\vec{p}+{}^6$He scattering at 200 MeV, we improve the VTC theory, using the eikonal approximation in addition to the $U_{pn_1} = U_{pn_2} = 0$ approximation and the adiabatic approximation. In the improved VTC theory, the A_y for ^{6}He is the same as that for ^{4}He. The $U_{pn_1} = U_{pn_2} = 0$ approximation is most essential among the three approximations. Using the CF model, we have confirmed that the $U_{pn_1} = U_{pn_2} = 0$ approximation is good in $0.9 \lesssim q \lesssim 2.4$ fm^{-1} for 200 MeV/nucleon, but good only near $q = 0.9$ fm^{-1} for 71 MeV/nucleon. In $0.9 \lesssim q \lesssim 2.4$ fm^{-1}, we predict $A_y(q)$ for $\vec{p}+{}^6$He scattering at 200 MeV from measured $A_y(q)$ for $\vec{p}+{}^4$He scattering at 200 MeV. This is a model-independent prediction in $0.9 \lesssim q \lesssim 2.4$ fm^{-1} ($20^\circ \lesssim \theta_{\rm c.m.} \lesssim 55^\circ$); see Fig. 3.

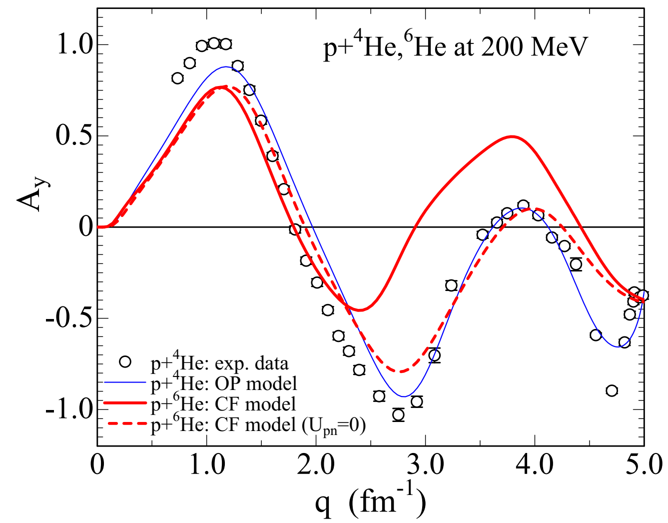

FIG. 7. q dependence of A_y for $\vec{p}+{}^6$He scattering at $E_{\rm lab} = 200$ MeV/nucleon. The solid line denotes a result of the CF-folding model, while U_{pn_1} and U_{pn_2} are switched off in the dashed line. The thin solid line is a result of the fitting for $\vec{p}+{}^4$He scattering at $E_{\rm lab} = 200$ MeV/nucleon. Open circles show the experimental data [7] for $\vec{p}+{}^4$He scattering. In $0.9 \lesssim q \lesssim 2.4$ fm^{-1}, open circles can be regarded as measured A_y for the $\vec{p}+{}^6$He scattering at $E_{\rm lab} = 200$ MeV/nucleon. Experimental data are taken from Ref. [7] for ^{4}He.

We have applied the cluster-folding (CF) model for $\vec{p}+{}^6$He scattering at 200 MeV, where the optical potential between $\vec{p}$ and ^{4}He is fitted to data for $\vec{p}+{}^4$He scattering at 200 MeV/nucleon; see Fig. 5. The CF model reproduces the differential cross section of $\vec{p}+{}^6$He scattering with no free parameter. We then predict A_y, as shown in Fig. 7. The solid line is our prediction based on the CF model, while the open circles are our model-independent prediction in $0.9 \lesssim q \lesssim 2.4$ fm^{-1}.

The ratio $|F(Q)|$ of measured differential cross sections for ^{6}He to that for ^{4}He is related to the wave function of ^{6}He. We have then determined the radius between ^{4}He and the center of mass of valence two neutrons. The radius is 3.54 fm. This is close to the radius 3.79 fm calculated with the ^{6}He density.

The Jensen-Shannon (JS) divergence [17] is new data analyses used by LIGO Scientific and Virgo Collaborations [18]. The present work is a first application of JS divergence in nuclear physics. Since the analysis is too new, we show it in Appendix.

We improved the JS divergence and applied two data on A_y for ^{4,6}He. As for $E_{\rm lab} = 71$ MeV/nucleon, the improved JS divergence shows that A_y for ^{6}He is close to that for ^{4}He, although the approximation (2) is not good. This is an interesting future work. We hope that new measurements will be made for ^{6}He $+\vec{p}$ scattering at 71 MeV/nucleon.

ACKNOWLEDGMENTS

We would like to thank Prof. Hiyama for providing the numerical data of the ^{6}He density, Dr. Toyokawa for pro-

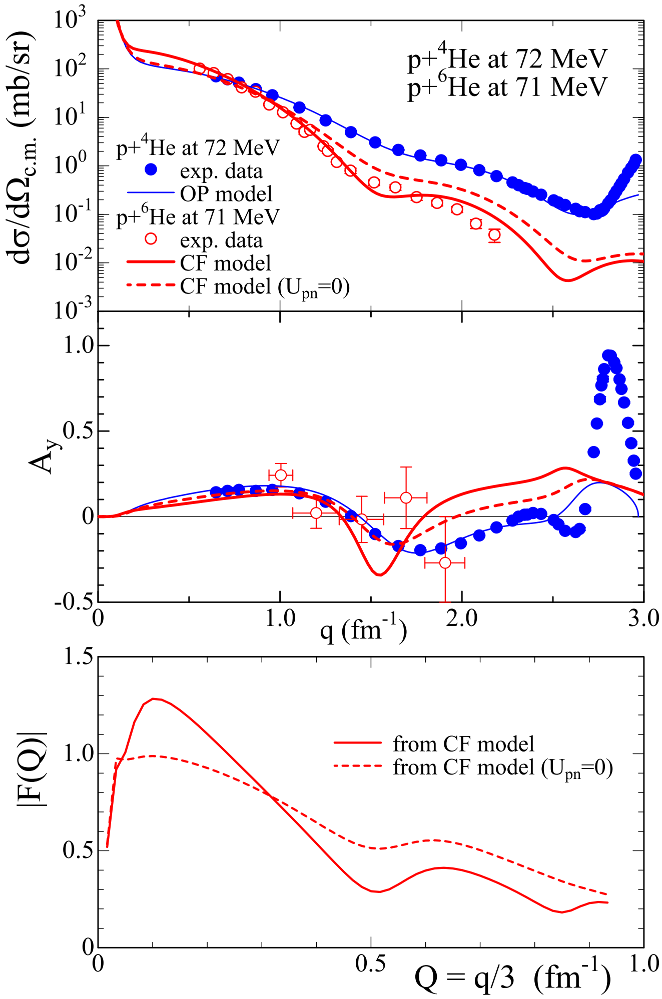

FIG. 8. q dependence of $d\sigma/d\Omega$ and A_y for $\vec{p}+{}^{4,6}\mathrm{He}$ scattering at $E_{\rm lab} \approx 71$ MeV/nucleon in the upper and middle panels and the form factor $|F(Q)|$ in the lower panel. The solid and dashed lines denote results of CF model with and without U_{pn_1} and U_{pn_2} for ^{6}He, respectively. The thin solid line denotes the result of fitting for ^{4}He. Data are taken from Refs. [5,15] for ^{6}He and from Ref. [16] for ^{4}He.

viding his code and Prof. Kouno for making comments, and Dr. Matsui for making a code.

APPENDIX: JENSEN-SHANNON DIVERGENCE FOR A_y FOR 71 MeV/NUCLEON

The Jensen-Shannon (JS) divergence consider two probabilities and make the comparison between their shapes quantitatively. We apply the JS divergence to A_y measured for $\vec{p}+{}^4\mathrm{He}$ scattering at $E_{\rm lab} = 72$ MeV/nucleon and that for $\vec{p}+{}^6\mathrm{He}$ scattering at $E_{\rm lab} = 71$ MeV/nucleon. This is a first application in nuclear physics. For this quantification, we start with two probability distributions, $p(q_i)$ and $p(q_i)$, having $0 \leqslant p(q_i) \leqslant 1$ and $0 \leqslant q(q_i) \leqslant 1$. The JS divergence is defined as [17]

$$D_{\rm JS}(p||q) = \sum_{i=1}^{N} D_{\rm JS}(q_i) \tag{A1}$$

with

$$D_{\rm JS}(q_i) = \frac{1}{2}\left[p(q_i)\ln\left(\frac{p(q_i)}{M(q_i)}\right) + q(q_i)\ln\left(\frac{q(q_i)}{M(q_i)}\right)\right], \tag{A2}$$

for $M(q_i) = (p(q_i)+q(q_i))/2$. The $D_{\rm JS}(p||q)$ satisfies

$$D_{\rm JS}(p||q) = D_{\rm JS}(q||p),$$
$$0 \leqslant D_{\rm JS}(p||q) \leqslant \ln rgb]0, 0, 12 = 0.693. \tag{A3}$$

The $D_{\rm JS}$ is finite; note that the word "divergence" is maintained for historical reasons. When the probability distributions are perfectly matched with each other, the $D_{\rm JS}$ becomes exactly zero. The $D_{\rm JS}$ becomes $\ln 2 = 0.693$, when there are no overlap between the probability distributions.

In the present data analysis, the number N of data is 5. The $\{p_i\}$ are a normalized distribution of measured $(A_y+1)/2$ for ^{4}He, while the $\{q_i\}$ are a normalized distribution of measured $(A_y+1)/2$ for ^{6}He. The reason why we take $(A_y+1)/2$ is that $0 \leqslant (A_y+1)/2 \leqslant 1$.

Our result $D_{\rm JS} \approx 0.0028$ is much smaller than $\ln 2 = 0.693$. This indicates that the shapes of the two probabilities are closed to each other. The average of $\{p_i\}$ ($\{q_i\}$) describes the magnitude M_4 (M_6) for ^{4}He (^{6}He). The results are $M_4 = 2.434$ and $M_6 = 2.539$. The two magnitudes are closed to each other, since the difference $(M_6 - M_4)/M_6$ is 4%.

When the two magnitudes are close to each other, we can improve the JS divergence as

$$D_{\rm JS}(p||q)M_{\rm av} = \sum_{i=1}^{N} D_{\rm JS}(q_i)M_{\rm av} \tag{A4}$$

with

$$D_{\rm JS}(q_i)M_{\rm av} \approx \frac{1}{2}\left[A_y^1(q_i)\ln\left(\frac{2A_y^1(q_i)}{A_y^1(p_i)+A_y^1(q_i)}\right) + A_y^1(p_i)\ln\left(\frac{2A_y^1(p_i)}{A_y^1(p_i)+A_y^1(q_i)}\right)\right], \tag{A5}$$

for the average $M_{\rm av} = (M_4+M_6)/2$ and $A_y^1(q_i) \equiv (A_y(q_i)+1)/2$. The $D_{\rm JS}(p||q)M_a$ describes the magnitude and the shape for two curves. Our result is $D_{\rm JS}(p||q)M_a = 0.007$ that is much smaller than the maximum $\ln 2 * M_a = 1.7236$. The improved JS divergence thus shows that measured A_y for ^{4,6}He are close to each other.

Now we neglect the data at $q = 1.71$ fm^{-1}. The result is $D_{\rm JS}(p||q)M_a = 0.002$. This value is much smaller than $D_{\rm JS}(p||q)M_a = 0.007$. The data at $q = 1.71$ fm^{-1} thus make the similarity between data for ^{4,6}He worse. We hope that new measurements will be made for $\vec{p}+{}^6\mathrm{He}$ scattering at 71 MeV/nucleon, particularly around $q = 1.71$ fm^{-1}.

[1] M. Toyokawa, K. Minomo, and M. Yahiro, Phys. Rev. C **88**, 054602 (2013).

[2] S. Watanabe *et al.*, Phys. Rev. C **89**, 044610 (2014).

[3] M. Hatano *et al.*, Eur. Phys. J. A **25**, 255 (2005).

[4] T. Uesaka, S. Sakaguchi, Y. Iseri, K. Amos, N. Aoi, Y. Hashimoto, E. Hiyama, M. Ichikawa, Y. Ichikawa, S. Ishikawa, K. Itoh, M. Itoh, H. Iwasaki, S. Karataglidis, T. Kawabata, T. Kawahara, H. Kuboki, Y. Maeda, R. Matsuo, T. Nakao, H. Okamura, H. Sakai, Y. Sasamoto, M. Sasano, Y. Satou, K. Sekiguchi, M. Shinohara, K. Suda, D. Suzuki, Y. Takahashi, M. Tanifuji, A. Tamii, T. Wakui, K. Yako, Y. Yamamoto, and M. Yamaguchi, Phys. Rev. C **82**, 021602(R) (2010).
[5] S. Sakaguchi *et al.*, Phys. Rev. C **84**, 024604 (2011).
[6] S. Chebotaryov *et al.*, PTEP **2018**, 053D01 (2018).
[7] G. A. Moss, *et al.*, Phys. Rev. C **21**, 1932 (1980).
[8] M. Burrows, C. Elster, S. P. Weppner, K. D. Launey, P. Maris, A. Nogga, and G. Popa, Phys. Rev. C **99**, 044603 (2019).
[9] R. Crespo and A. M. Moro, Phys. Rev. C **76**, 054607 (2007).
[10] M. Gennari, M. Vorabbi, A. Calci, and P. Navratil, Phys. Rev. C **97**, 034619 (2018).
[11] R. C. Johnson, J. S. Al-Khalili, and J. A. Tostevin, Phys. Rev. Lett. **79**, 2771 (1997).
[12] R. C. Johnson, J. Phys. G: Nucl. Part. Phys. **24**, 1583 (1998).
[13] R. J. Glauber, *Lectures in Theoretical Physics* (Interscience, New York, 1959), Vol. 1, p.315.
[14] M. Yahiro, K. Minomo, K. Ogata, and M. Kawai, Prog. Theor. Phys. **120**, 767 (2008).
[15] A. A. Korsheninnikov *et al.*, Nucl. Phys. A **617**, 45 (1997).
[16] S. Burzynski, J. Campbell, M. Hammans, R. Henneck, W. B. Lorenzon, M. A. Pickar, and I. Sick, Phys. Rev. C **39**, 56 (1989).
[17] J. Lin, IEEE Transactions on Information Theory **37**, 145 (1991).
[18] B. P. Abbott *et al.* (LIGO Scientific and Virgo Collaborations), Phys. Rev. X **9**, 031040 (2019).
[19] E. Hiyama, M. Kamimura, T. Motoba, T. Yamada, and Y. Yamamoto, Phys. Rev. C **53**, 2075 (1996).
[20] E. Hiyama, Y. Kino, and M. Kamimura, Prog. Part. Nucl. Phys. **51**, 223 (2003).
[21] N. Yamaguchi, S. Nagata, and T. Matsuda, Prog. Theor. Phys. **70**, 459 (1983).
[22] S. Nagata, M. Kamimura, and N. Yamaguchi, Prog. Theor. Phys. **73**, 512 (1985).
[23] N. Yamaguchi, S. Nagata, and J. Michiyama, Prog. Theor. Phys. **76**, 1289 (1986).
[24] T. Hamada and I. Johnston, Nucl. Phys. **34**, 382 (1962).